

Multiple Sources toward the High-mass Young Star S140 IRS 1

Miguel A. Trinidad¹ José M. Torrelles², Luis F. Rodríguez³, Salvador Curiel⁴

trinidad@astro.ugto.mx

ABSTRACT

S140 IRS1 is a remarkable source where the radio source at the center of the main bipolar molecular outflow in the region is elongated perpendicular to the axis of the outflow, an orientation opposite to that expected if the radio source is a thermal jet exciting the outflow. We present results of 1.3 cm continuum and H₂O maser emission observations made with the VLA in its A configuration toward this region. In addition, we also present results of continuum observations at 7 mm and re-analyse observations at 2, 3.5 and 6 cm (previously published). IRS 1A is detected at all wavelengths, showing an elongated structure. Three water maser spots are detected along the major axis of the radio source IRS 1A. We have also detected a new continuum source at 3.5 cm (IRS 1C) located $\simeq 0''.6$ northeast of IRS 1A. The presence of these two YSOs (IRS 1A and 1C) could explain the existence of the two bipolar molecular outflows observed in the region. In addition, we have also detected three continuum clumps (IRS 1B, 1D and 1E) located along the major axis of IRS 1A. We discuss two possible models to explain the nature of IRS 1A: a thermal jet and an equatorial wind.

Subject headings: YSOs—ISM: individual (S140 IRS 1) — ISM: jets and outflows — masers — stars: formation

¹Departamento de Astronomía, Universidad de Guanajuato, Apdo. Postal 144, Guanajuato, Gto. 36240, México

²Instituto de Ciencias del Espacio (CSIC) and Institut d'Estudis Espacials de Catalunya, Facultat de Física, Planta 7a, Universitat de Barcelona, Av. Diagonal 647, 08028 Barcelona, Spain

³Centro de Radioastronomía y Astrofísica, (UNAM), Apdo. Postal 3-72 (Xangari) 58089 Morelia, Michoacán, México

⁴Instituto de Astronomía, UNAM, Apdo. Postal 70-264, D.F. 04510, México

1. Introduction

The process of low-mass star formation is reasonably well understood. The accepted model (e.g., Shu et al. 1987) requires a disk-YSO-outflow system (*YSO: young stellar object*), and it has been supported by theoretical and observational results (e.g. Evans, 1999 and references therein). In addition, bipolar molecular outflows associated with low-mass stars are believed to be driven by their jets, that can be observed at sub-arcsec scales and this constitute the best evidence of collimation at the smallest scales now known (e.g. Anglada 1996). However, the process of high-mass star formation is not well understood yet. In fact, although molecular outflows seem to be also common among high-mass stars (Gómez et al. 1999, Zhang et al. 2001, Ridge & Moore, 2001; Beuther et al. 2002, Shepherd 2005), there is still a deficit in the detection of circumstellar disks and jets associated with massive YSOs (e.g., Cepheus A HW2: Rodríguez et al. 1994; Patel et al. 2005; Curiel et al. 2006; IRAS 20126+4104: Cesaroni et al. 1999; Trinidad et al. 2005; Sridharan et al. 2005; AFGL 490: Schreyer et al. 2006; G24.78+0.08: Beltrán et al. 2006). In spite of these studies, it is not clear whether molecular outflows in massive YSOs are also driven by collimated jets as low-mass stars do. Therefore, studies of individual high-mass YSOs are very important to address these issues, but their identification is more difficult than in the case of low-mass objects. Firstly, the spatial density of massive objects is smaller and we need to go to greater distances to increase the known sample and build statistical significance, and second, they are formed in dense clusters and sub-arcsecond angular resolution observations are required to isolate them.

The star-forming region, S140 IRS, is located in the molecular cloud L1204 at a distance of 910 pc (Crampton & Fisher, 1974). In this region, there is a group of at least three ZAMS B stars (IRS 1, IRS 2, IRS 3; Beichman et al. 1979), with a total luminosity of $\sim 3 \times 10^3 L_{\odot}$ (Lester et al. 1986), with IRS 1 being the brightest one. In addition, a CO bipolar outflow extended along the northwest-southeast direction has been observed in the region by Hayashi et al. (1987). Minchin et al. (1993) found that the blue and redshifted lobes of the CO bipolar outflow have position angles of $\sim 160^{\circ}$ and $\sim 340^{\circ}$, respectively. On the other hand, K band (2.0-2.3 μm) and H₂ observations have revealed two bipolar outflows in the region (Preibisch & Smith 2002 and Weigelt et al. 2002), one of them with an orientation similar to the CO outflow (160/340 $^{\circ}$) and the other one in the 20/200 $^{\circ}$ direction. Both bipolar outflows seem to be centered on IRS 1. The region S140 IRS has also been studied at the infrared and optical bands (Eiroa et al. 1993), NH₃ lines (Verdes-Montenegro et al. 1989), and radio continuum emission (Schwartz 1989, Evans et al. 1989). More recently, Hoare (2006) has observed IRS 1 at 6 cm during three epochs with MERLIN, and shows, through a very detailed analysis that it is highly elongated in the northeast-southwest direction, and also proposes that the radio continuum traces an ionized equatorial wind driven by

radiation pressure from the central star and oriented in the northeast-southwest direction, perpendicular to the CO bipolar outflow. In addition, water maser emission has also been detected toward the S140 IRS region (e.g. Tofani et al. 1995, Lekht et al. 1993, Lekht & Sorochenko 2001, Trinidad et al. 2003).

In this paper, we report and discuss new high angular resolution observations of 1.3 cm continuum and water maser emission toward the S140 IRS region carried out with the Very Large Array (VLA) in the A configuration. In order to present a full study of IRS 1, we have also analyzed 7 mm continuum observations (VLA data archive; see also Gibb & Hoare, 2007) and re-analyzed VLA centimeter continuum observations (previously published by Schwartz 1989 and Tofani et al. 1995). We describe the observations in §2 and present the results in §3. In Section §4, we discuss the nature of the multiple continuum sources that we detect in the region, while our main conclusions are summarized in §5.

2. Observations

The observations toward the S140 IRS region were made with the VLA of the National Radio Astronomy Observatory (NRAO)¹ in its A configuration on 1999 June 29. We observed simultaneously 1.3 cm continuum and water maser emission. We used two different bandwidths, one of 25 MHz with seven channels for the continuum and another one of 3.125 MHz with 63 channels for the maser line emission. Both the right and left circular polarizations were sampled in the above two different bandwidths, which were averaged in order to improve the sensitivity. The broad bandwidth for the continuum observations was centered at 22285.080 MHz, while the narrow bandwidth for the line observations was centered at the frequency of the H₂O 6₁₆ → 5₂₃ maser line (rest frequency 22235.080 MHz) with $V_{LSR} = -9.0$ km s⁻¹, covering from -28 to 10 km s⁻¹ in velocity. The absolute amplitude calibrator was 3C 286 with an adopted flux density of 2.51 Jy, while the phase calibrator was B2021+614 with a bootstrapped flux density of 2.14 ± 0.05 Jy. The water maser line and continuum data were reduced and calibrated using the standard techniques using the NRAO AIPS software package. After the first calibration, we searched the narrow bandwidth data for the spectral channel with the strongest water maser emission and then its signal was self-calibrated in phase and amplitude. We then cross-calibrated the data applying the phase and amplitude corrections to both the narrow and the broad bandwidths. In this way, the atmospheric and instrumental errors at high frequencies on long baselines were removed

¹ The NRAO is operated by Associated Universities Inc., under cooperative agreement with the National Science Foundation.

(see for details Reid & Menten 1990, Torrelles et al. 1996) and the signal-to-noise ratio was improved.

We also used the data set at 7 mm from the VLA data archive (see also Gibb & Hoare, 2007). In addition, we re-analyzed continuum observations at 2, 3.5 and 6 cm, which have been previously published (see Table 1). All observations were carried out in the A configuration. We recalibrated these data sets and made new contour maps using the current procedures of AIPS. We used the physical parameters derived from these new contour maps for the discussion in this paper. Contour maps at 2 and 6 cm and their measured physical parameters are consistent with those published before by Schwartz (1989). However, the flux density estimated at 3.5 cm is different (about 50% lower) to that reported by Tofani et al. (1995), probably due to a typo.

3. Observational Results

Figure 1 shows the contour maps of S140 IRS 1 at centimeter wavelengths (1.3, 2.0, 3.5 and 6.0 cm). Given that other condensations are also detected around S140 IRS 1, hereafter, we will refer to S140 IRS 1 as S140 IRS 1A or only IRS 1A for clarity. This source appears spatially resolved at all wavelengths. The physical parameters of the radio source IRS 1A (position, flux density, deconvolved angular size and position angle) were obtained from elliptical Gaussian fits using the AIPS task IMFIT and are given in Table 2. Contour maps at 1.3 and 2 cm have similar angular resolution ($\sim 0''.1$) and were made with natural- and uniform-weighting, respectively. On the other hand, contour maps at 3.5 and 6 cm have an angular resolution of $\sim 0''.3$ (Figure 1). For the map at 3.6 cm a Gaussian taper of 850 $\kappa\lambda$ was used, while at 6 cm a ROBUST = -1 parameter (Briggs 1995) of the AIPS task IMAGR was used.

In all contour maps (Figure 1), IRS 1A shows a general elongated morphology in the northeast-southwest direction, similar to the orientation of the bipolar outflow observed in H₂ toward IRS 1A in the 20°/200° direction (Preibisch & Smith 2002). In addition, our contour map at 1.3 cm with angular resolution of $\simeq 0''.08$ (ROBUST = 0 parameter was used in order to optimize the compromise between the signal-to-noise ratio and the angular resolution) shows a second peak, at a level of 4σ , located about $0''.13$ to the southwest from IRS 1A (Figure 2). We will refer to this peak as IRS 1B. Furthermore, three other continuum peaks (that we will refer as IRS 1C, IRS 1D and IRS 1E), are also observed at 3.5 cm with an angular resolution of $0''.25$ (Figure 2). IRS 1C is located $\sim 0''.6$ to the northeast of IRS 1A (Figure 2) and is also detected at 2 cm with an angular resolution of $\sim 0''.15$. IRS 1D and IRS 1E are located $\sim 0''.35$ to the northeast and southwest of IRS 1A, respectively. Their

main observed parameters are given in Table 2.

On the other hand, IRS 1A is detected at 7 mm (Figure 3; flux density and deconvolved size are given in Table 2) while this is not the case for IRS 1B, 1C, 1D or 1E. Although the 7 mm continuum emission is also elongated in the northeast-southwest direction as the centimeter emission (1.3, 2, 3.5 and 6 cm), they do not have, within the error, the same position angle (the millimeter emission has a position angle of $\sim 61^\circ$, while the centimeter emission has a position angle of $\sim 44^\circ$). These results are consistent with those found very recently by Gibb and Hoare (2007).

The water maser emission toward S140 IRS was in a period of minimum activity during our VLA observations and we only detect three water maser features spatially associated with IRS 1A (Figure 1). One of these maser features, with redshifted velocity with respect to the molecular cloud velocity ($\sim -6.5 \text{ km s}^{-1}$, Zhou et al. 1993), is located close ($0''.1$) to the IRS 1A continuum emission peak at 1.3 cm, while the other two maser features, with blueshifted velocity with respect to the molecular cloud velocity, are located $\sim 0''.5$ and $\sim 0''.7$ to the southwest of IRS 1A, respectively (see Fig. 1 and Table 3). Figure 9 from Trinidad et al. (2003) shows that the water maser emission toward S140 IRS was stronger (up to 46 Jy with at least seven features) a month before the VLA observations presented here. The position, velocity, and flux density of the three detected VLA water maser features are given in Table 3.

4. Discussion

The elongated morphology of the IRS 1A is evident in the contour maps at all centimeter wavelengths (1.3, 2, 3.5, and 6 cm), suggesting a jet-like nature (see Figure 1), similar to other possible radio jets associated with massive YSOs (e.g., Claussen et al. 1994, Rodríguez et al. 1994, Torrelles et al. 1997, Hofner et al. 1999, Gibb et al. 2003, Trinidad et al. 2003, 2005, Curiel et al. 2006; see Hoare 2006 and references therein). However, Hoare (2006), based on very detailed 6 cm continuum multiepoch observations with MERLIN, has proposed that the continuum emission is produced by an equatorial wind. We discuss both of these possibilities below.

4.1. IRS 1A: A Thermal Radio Jet?

In order to investigate whether or not IRS 1A is a thermal jet, we have calculated, following the formalism of Reynolds (1986), the dependence of the flux density and the

deconvolved angular size of the major axis of the jet with the frequency. For the case of a thermal jet with constant velocity, temperature, and ionization fraction, the dependence of the flux density with the frequency is $S_\nu \propto \nu^\alpha$ ($\alpha = 1.3 - 0.7/\epsilon$; equation 14 of Reynolds 1986), while that for the deconvolved angular size of the major axis is $\theta_{maj} \propto \nu^\beta$ ($\beta = -0.7/\epsilon$). Under this formalism, ϵ is the power-law index that describes the dependence of the jet half-width, w (perpendicular to the major axis of the jet), as a function of the distance from the origin. For a conical jet, $\epsilon = 1$, then, $\alpha = 0.6$ and $\beta = -0.7$.

From the multiepoch observations at 6 cm (Hoare 2006), it is known that the flux density of IRS 1A is not variable with time. Assuming that the flux density of IRS 1A has not changed significantly with time also at other wavelengths (the observations were made with a time span of about 12 years; see Table 1), we roughly estimate a spectral index of $\alpha = 0.5 \pm 0.1$ by using the flux densities at 0.7, 1.3, 2, 3.6, and 6 cm (see Figure 4). In addition, we also estimate the dependence of the angular size of the major axis of IRS 1A with frequency, where the parameter is $\beta = 0.98 \pm 0.06$ (see Figure 4). Both indices, α and β , seem to be consistent with free-free emission in the wavelength range 0.7–6 cm, produced either by a conical collimated ionized jet ($\epsilon = 2/3$, "standard" collimated jet) or by a conical ionized jet ($\epsilon = 1$, "standard" spherical jet) (see Table 1 of Reynolds 1986). On the other hand, using the flux density of IRS 1A at 1.3 cm (this work) and that at 6 cm obtained with MERLIN observations (Hoare 2006), a spectral index of about 0.6 ± 0.1 is obtained, which is consistent with that estimated using only VLA observations. In this way, we also note that the flux density and angular diameter of IRS 1A as measured with the VLA, with an angular resolution of about $0''.35$, and those measured with MERLIN (Hoare 2006), with an angular resolution of about $0''.11$, are consistent within 25–30%. This result shows that changes of the angular diameter of the source is not due to an effect of angular resolution; that is, the larger angular size measured at low frequencies is not an effect of lower angular resolution than at higher frequencies.

Under the assumption that IRS 1A is a thermal jet, we can also estimate the ionized mass-loss (\dot{M}) and momentum rate (\dot{P}) deposited by IRS 1A into the ambient medium. Following Reynolds (1986) and using equation 3 given by Beltrán et al. (2001), for a pure hydrogen jet with constant velocity and ionization fraction, we have

$$\left(\frac{\dot{M}}{10^{-6} M_\odot \text{yr}^{-1}} \right) = 0.108 \left[\frac{(2 - \alpha)(0.1 + \alpha)}{1.3 - \alpha} \right]^{3/4} \left[\left(\frac{S_\nu}{mJy} \right) \left(\frac{\nu}{10GHz} \right)^{-\alpha} \right]^{3/4} \left(\frac{V}{200km s^{-1}} \right) \\ \times \left(\frac{\nu_m}{10GHz} \right)^{0.75\alpha - 0.45} \left(\frac{\theta_o}{rad} \right)^{3/4} (\sin i)^{-1/4} \left(\frac{d}{kpc} \right)^{3/2} \left(\frac{T}{10^4 K} \right)^{-0.075}, \quad (1)$$

where α is the spectral index, S_ν is the observed flux density at frequency ν , V is the terminal velocity of the jet, ν_m is the turnover frequency, θ_o is the opening angle, i is the jet axis

inclination, d is the distance to the source and T is the electron temperature. The opening angle is approximately estimated using $\theta_o = 2 \tan^{-1}(\theta_{min}/\theta_{maj})$.

Then, assuming a inclination angle of the jet axis relative the line of sight, $i = 60^\circ$, a distance of 910 pc, an electron temperature of 10^4 K, a lower limit for ν_m ($= 22.2$ GHz), and a terminal velocity of ~ 500 km s $^{-1}$, we determine the mass-loss (\dot{M}) and momentum rate (\dot{P}) deposited by IRS 1A into the ambient medium as $\sim 9 \times 10^{-7}$ M $_{\odot}$ yr $^{-1}$ and $\sim 4.5 \times 10^{-4}$ M $_{\odot}$ yr $^{-1}$ km s $^{-1}$, respectively. These values are similar to those obtained for the thermal jets associated with other massive YSOs (e.g Cep A W2 and HH 80). On the other hand, using the correlation (momentum rate versus radio continuum luminosity) given by Anglada (1996) to estimate the momentum rate, we find a value about two order of magnitude larger than that estimated using the formalism of Reynolds. This result suggests that Anglada’s correlation is valid only for low luminosity objects and cannot be extrapolated to high luminosity sources.

We have also detected four condensations almost aligned along the major axis of the IRS 1A (see Figure 2). One continuum peak (IRS 1B) is detected at 1.3 cm, while the other three continuum peaks (IRS 1C, 1D, 1E) are detected at 3.5 cm. As IRS 1B is detected only at 1.3 cm (although IRS 1B and 1E are located to the southwest of IRS 1A, both continuum peaks are not spatially coincident), we are not able to estimate its spectral index, which could have helped to investigate whether it is a condensation ejected by IRS 1A or, alternatively, an independent source. The continuum peaks IRS 1D and 1E are almost symmetrically located with respect to IRS 1A (see Figure 2) and both condensations have similar peak flux densities, which could suggest that they are condensations ejected by IRS 1A, as could be expected for a thermal jet. Multiepoch observations (e.g at 3.5 cm) to measure possible proper motions of IRS 1D and 1E could test if these are condensations ejected by the jet. On the other hand, the condensation IRS 1C does not have a counterpart on the symmetrically opposite side as in the case of the pair formed by 1D and 1E. In addition, IRS 1C appears misaligned with respect to the 1D-IRS 1A-1E system (see Figure 2). Then, if IRS 1C was also ejected by the jet IRS 1A, this could indicate that IRS 1A is precessing. Alternatively, IRS 1C could be an independent source. In this way, IRS 1C seems to coincide spatially, within the positional error, with the clump NE-N detected by Hoare (2006) at 6 cm wavelength. Using the peak flux densities at 3.5 (this work) and 6 cm (Hoare 2006), we have roughly estimated a spectral index for IRS 1C of ~ 0.4 , which suggest that the continuum emission of IRS 1C is being produced by partially-thick thermal free-free emission. In addition, Hoare (2006) has reported possible proper motion of the NE-N clump with a tangential velocity of 120 km s $^{-1}$ moving toward the east. However, due to this high value of the velocity, Hoare (2006) opens the possibility that the proper motion is not due to real physical motion but due to a travelling illuminating wave.

The overall radio continuum properties of IRS 1A indicate that it could be a thermal jet associated with a high-mass YSO. In addition, the position angle of the elongated structure at cm wavelengths ($\sim 44^\circ$; Table 2) suggests that IRS 1A could be the driving source of the bipolar molecular outflow seen in H_2 in the direction $20^\circ/200^\circ$. Under this scenario and assuming that the condensation IRS 1C is an independent source, we speculate that this newly detected source (IRS 1C) could be the driving source of the other bipolar molecular outflow observed in the direction $160^\circ/340^\circ$. If this is the case, two close, independent and almost perpendicular jets could be the driving sources of the two bipolar outflows observed in the region (see Figure 2). Perpendicular thermal jets have been observed in low-mass star forming regions (e.g. HH 111, Reipurth et al. 1999).

In addition, all water maser features detected toward S140 IRS are associated with IRS 1A, assuming that IRS 1E is not a stellar object but ejected from IRS 1A (see Figure 1 and 2). The estimated mass for IRS 1A, assuming that the masers are bound gravitationally, is $\geq 60 M_\odot$, which is greater than the mass estimated from its luminosity ($\sim 10 M_\odot$). This result indicates that the water maser features are not associated with a circumstellar disk, instead, the water masers are tracing unbound motions, which is consistent with IRS 1A being a thermal jet. Further observations with high angular resolution and proper motion studies will be needed to study in detail the three-dimensional (spatio-kinematical) distribution of the water masers in the region, which will help to understand the nature of the IRS 1A and possibly discriminate between the thermal jet and equatorial wind models (see below).

4.2. IRS 1A: An Equatorial Wind?

Using high angular resolution multiepoch observations at 6 cm toward IRS 1A, Hoare (2006) proposes that IRS 1A is an equatorial wind driven by radiation pressure from a central star and inner disk acting on the gas in the surface layers of the disk, and perpendicular to the CO bipolar outflow observed in the direction $160^\circ/340^\circ$. This scenario is supported by two facts. First, the location and extension perpendicular to the major axis of IRS 1A of a small scale monopolar near-IR reflection nebula at the base of the blueshifted lobe of the molecular outflow, and second, the small outward proper motion of a continuum clump in the direction $160^\circ/340^\circ$ as would be expected for a jet.

The results of Hoare are opposed to the picture of the multiple jets described above for IRS 1A. However, our observational results could be also consistent with IRS 1A being an equatorial wind. As mentioned above (§ 4.1), there are two condensations (IRS 1D and 1E) located symmetrically on opposite sides of the central source, IRS 1A, and under the

equatorial wind model, IRS 1D and 1E could be tracing the outer border of the wind within a disk with diameter of ~ 650 AU.

Unfortunately, with the present data we cannot discriminate between the two proposed models for IRS 1A (jet versus equatorial wind). However, we note that the presence of the outflow in the $20^\circ/200^\circ$ direction (in addition to the outflow in the $160^\circ/340^\circ$ direction), requires at least two independent powering YSOs in the region. In this way, within the equatorial wind scenario IRS 1A would be the exciting source of the $160^\circ/340^\circ$ outflow (as proposed by Hoare 2006), while the new detected source IRS 1C would power the $20^\circ/200^\circ$ outflow.

Additional observations are required to discriminate in a more definitive way between the equatorial wind and the thermal jet scenarios. Any detection of large proper motions (hundred of km s^{-1}) in the IRS 1D and 1E condensations in the northeast-southwest direction would favor the jet hypothesis. This test would require sensitive, high angular resolution continuum observations over several years. On the other hand, the study of the high velocity molecular gas in the vicinity of the source IRS 1A could reveal the wide angle outflow expected from an equatorial wind. Any detection, with high angular resolution observations, of molecular gas correlated with the radio continuum source could trace the neutral part of the disk and also provide strong evidence favoring the equatorial wind scenario. In addition, as we have mentioned before, proper motion studies of the water masers observed in this region could be a powerful tool to discriminate between both models. On the other hand, with the present theoretical models (e.g. Drew et al. 1998; Lugo et al. 2004), we cannot also discriminate between jet and equatorial wind models. However, we think that in an equatorial wind model the angular diameter might be less sensitive to the frequency of observation than in an jet model. In any case, more detailed theoretical studies will be necessary to address this important issue.

5. Conclusions

We have presented results of 1.3 cm continuum and water maser emission observations made with the VLA in its A configuration toward the S140 IRS region. We have also re-analyzed continuum observations at 0.7, 2, 3.5, and 6 cm.

We observed IRS 1A at all wavelengths (0.7, 1.3, 2, 3.5, and 6 cm) and also detected four new continuum peaks (IRS 1B, 1C, 1D and 1E). IRS 1B is only detected at 1.3 cm, while IRS 1C, 1D and 1E are detected at 3.5 cm. IRS 1C, located $\sim 0''.6$ to the northeast of IRS 1A, seems to be an independent source, while IRS 1D and 1E, located symmetrically with respect

to IRS 1A, seem to be condensations associated with IRS 1A. Under this scenario, IRS 1A is not a single source, but a possible binary formed by IRS 1A and 1C. These two YSOs could explain the excitation of the two large bipolar molecular outflows observed toward S140 IRS1. We have also detected three water masers toward IRS 1 that most probably are tracing unbound motions and are associated with the bipolar molecular outflow in the northeast-southwest direction.

In order to understand the nature of IRS 1A, we have analyzed two scenarios: the thermal jet model and the equatorial wind model. The elongated morphology and spectral indices, α and β , of the continuum emission in the 0.7 – 6 cm wavelength range, are consistent with IRS 1A being a thermal jet. However, a photoevaporated disk (Hoare 2006, Gibb & Hoare 2007) could produce a similar morphology and spectral energy distribution. Proper motion measurements of the detected continuum clumps IRS 1D and 1E would help to discriminate between these two scenarios (jet versus equatorial wind). In addition, proper motion measurements of the detected water masers would also be very valuable in this sense.

M.A.T. acknowledges the support from CONACyT grant 46157-E. J.M.T. acknowledges partial financial support from the Spanish grant AYA2005-08523-C03

REFERENCES

- Anglada, G. 1996, ASP Conference Series (Radio Emission from Stars and the Sun), eds. A.R. Taylor and J.M. Paredes, 93, 3
- Beltrán, M. T., Cesaroni, R., Codella, C., Testi, L., Furuya, R. S., Olmi, L. 2006, *Nature*, 443, 427
- Beltrán, M. T., Estalella, R. Anglada, G. Rodríguez, L.F., & Torrelles, J.M. 2001, *AJ*, 121, 1556
- Beichman, C. A., Becklin, E. E., & Wynn-Williams, C. G. 1979, *ApJ*, 232, L47
- Briggs, D. 1995, Ph.D. thesis, New Mexico Inst. Mining and Technol.
- Cesaroni, R., Felli, M., Jenness, T., Neri, R., Olmi, L., Robberto, M., Testi, L., & Walmsley, C.M. 1999, *A&A*, 345, 949
- Cohen, R. J., Rowland, P. R., & Blair, M. M. 1984, *MNRAS*, 210, 425
- Crampton, D., & Fisher, W. A. 1974, *Pub. Dom. Ap. Obs.*, 14, 12

- Curiel, S., Rodríguez, L. F., Moran, J. M., & Cantó, J. 1993, *ApJ*, 415, 191
- Curiel, S., Ho, P. T. P., Patel, N. A., Torrelles, J. M., Rodríguez, L. F., Trinidad, M. A., Cantó, J., Hernández, L., Gómez, J. F., Garay, G., & Anglada, G. 2006, *ApJ*, 638, 878
- Eiroa, C., Lenzen, R., Miranda, L. F., Torrelles, J. M., Anglada, G., Estalella, R. 1993, *AJ*, 106, 613
- Evans, N. J. II, Mundy, L. G., Kutner, M. L., & DePoy, D. L. 1989, *ApJ*, 346, 212
- Evans, N. J. II 1999, *ARA&A*, 37, 311
- Gibb, A. G. and Hoare, M. G., 2007, *MNRAS*, in press.
- Gómez, Y., Rodríguez, L. F., & Martí, J. 1995, *ApJ*, 453, 268
- Gómez, J. F., Sargent, A. I., Torrelles, J. M., Ho, P. T. P., Rodríguez, L. F., Cantó, J., Garay, G. 1999, *ApJ*, 514, 287
- Hayashi, M., Hasegawa, T., Omodaka, T. Hayashi, S.S. and Miyawaki, R. 1987, *ApJ*, 312, 327
- Hoare, M.G. 2006, *ApJ*, 649, 856
- Lekht, E. E., Likhachev, S. F., Sorochenko, R. L., and Strel’Nitskii, V. S. 1993, *ARep*, 37, 367L
- Lekht, E. E. & Sorochenko, R. L. 2001, *ARep*, 45, 113L
- Lester, D. F., Harvey, P. M., Joy, M., & Ellis, H. B. Jr. 1986, *ApJ*, 309, 80
- Lugo, J., Lizano, S., & Garay, G. 2004, *ApJ*, 614, 807
- Martí, J., Rodríguez, L.F, & Reipurth, B. 1995, *ApJ*, 449, 184
- Minchin, N. R., White, G. J., & Padman, R. 1993, *A&A*, 277, 595
- Preibisch, T. and Smith, M.D. 2002 *A&A*, 383, 540
- Reid, M.J. and Moran, J.M. 1981, *ARA&A*, 19, 231
- Reid, M. J., and Menten, K. M. 1990, *ApJ*, 360, L51
- Reipurth, B., Yu, K. C., Rodríguez, L.F., Heathcote, S., & Bally, J. 1999, *A&A*, 352, 83L

- Ridge, N.A. & Moore, T.J.T. 2001, *A&A*, 378, 495
- Rodríguez, L. F., Garay G., Curiel, S. Ramírez, S., Torrelles J. M., Gómez, Y., & Velázquez, A. 1994, *ApJ*, 430, L65
- Reynolds, S. P. 1986, *ApJ*, 304, 713
- Schreyer, K., Semenov, D., Henning, Th., & Forbrich, J. 2006, *ApJ*, 637, 129
- Schwartz, P. R. 1989, *ApJ*, 338, L25
- Shepherd, D. 2005, *IAUS*, 227, 237
- Shu, F. H., Adams, F. C., & Lizano, S. 1987, *ARA&A*, 25, 23
- Sridharan, T. K., Williams, S. J., & Fuller, G. A. 2005, 631, 73
- Tofani, G., Felli, M., Taylor, G. B., & Hunter, T. R. 1995, *A&AS*, 112, 299
- Torrelles, J.M., Gómez, J. F., Rodríguez L. F., Curiel S., Ho, P. T. P., & Garay, G. 1996, *ApJ*, 457, L107
- Trinidad, M. A., Rojas, V., Plascencia, J.C., Ricalde, A., Curiel, S., & Rodríguez, L.F. 2003, *Rev. Mexicana Astron. Astrofis.*, 39, 311
- Trinidad, M. A., Curiel, S., Migenes, V., Patel, N., Torrelles, J. M., Gómez, J. F., Rodríguez, L. F., Ho, P. T. P. & Cantó, J. 2005, *AJ*, 130, 2206
- Verdes-Montenegro, L., Torrelles, J. M., Rodríguez, L. F., Anglada, G., López, R., Estalella, R., Cantó, J., Ho, P. T. P. 1989, *ApJ*, 346, 93
- Weigelt, G., Preibisch, Th., Schertl, D., Balega, Y. Y., & Smith, M. D. 2002, *A&A*, 381, 905
- Zhang, Q., Hunter, T.R., Brand, J., Sridharan, T.K., Molinari, S., Kramer, M.A., & Cesaroni, R. 2001, *ApJ*, 552, 167L
- Zhou, S., Evans, N.J. II, Mundy, L.G., & Kutner, M.L. 1993, *ApJ*, 417, 613

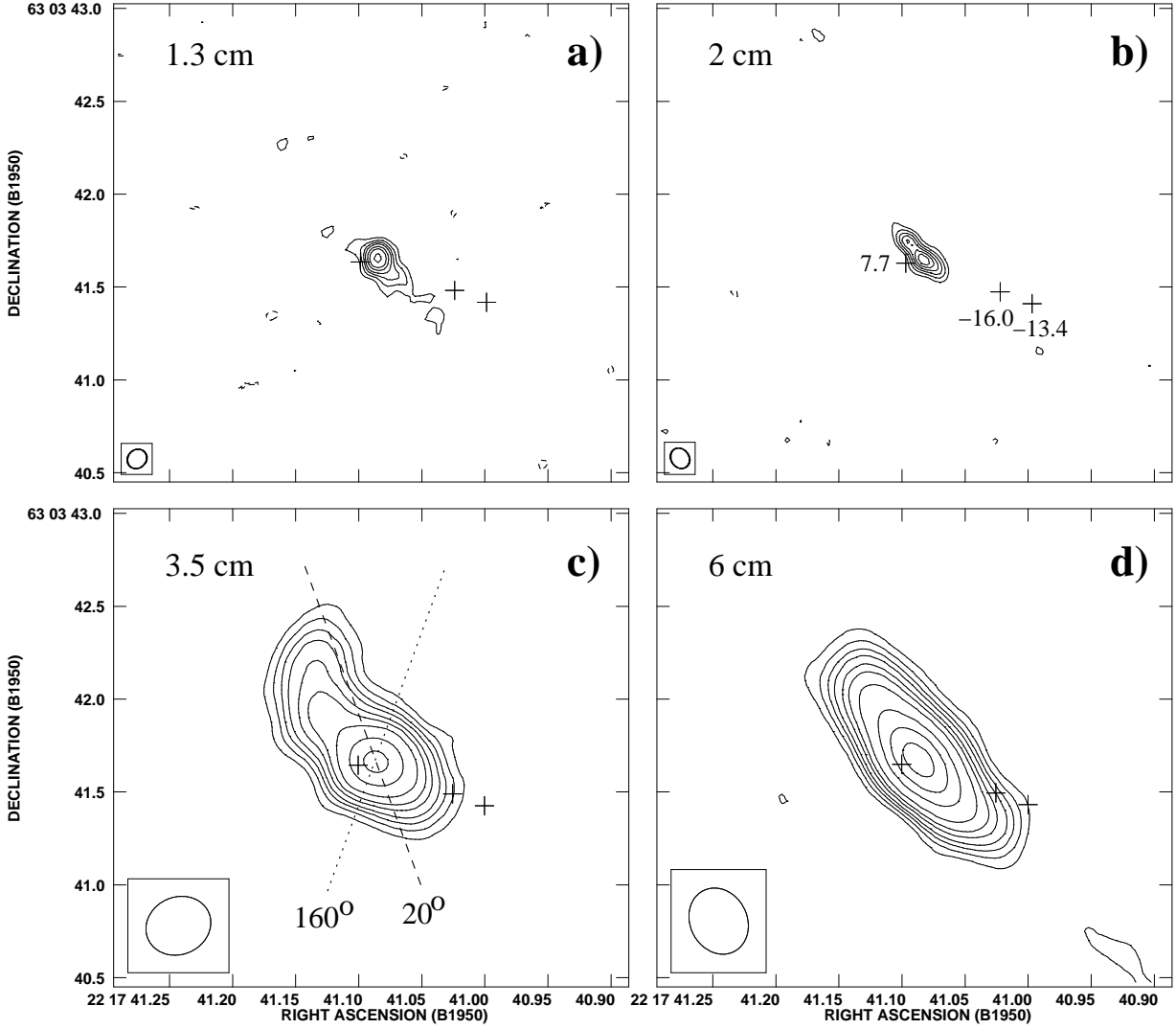


Fig. 1.— Radio continuum contour maps showing consistently an elongated structure for S140 IRS 1A at several wavelengths. Contours are $-3, 3, 5, 7, 9, 12, 15$ and 20 (*panel a*: 1.3 cm; beam $0''.11 \times 0''.09$), $-3, 3, 5, 7, 9, 11$, and 13 (*panel b*: 2 cm; beam $0''.12 \times 0''.10$), $-3, 3, 5, 7, 9, 12, 15, 20, 30$ and 40 (*panel c*: 3.5 cm; beam $0''.36 \times 0''.31$), and $-3, 3, 5, 7, 9, 12, 15, 20, 30, 40$ and 50 (*panel d*: 6 cm; beam $0''.37 \times 0''.31$) times 200, 170, 43 and $40 \mu\text{Jy beam}^{-1}$, respectively, the rms noise of the maps. In all maps the beam is shown in the lower left corner. In order to make all continuum peaks of IRS 1A coincide, we have applied an offset of $(\alpha, \delta) = (-0^s.0017, -0''.007)$, $(+0^s.0017, +0''.009)$, and $(+0^s.0016, +0''.014)$ to the position of IRS 1A at 2, 3.5 and 6 cm, respectively. The crosses show the position of the water masers detected in the region with their LSR velocity values (km s^{-1}) indicated in panel b. The dashed and dotted lines in panel c indicate, respectively, the axes of the H_2 jet and CO outflow seen on large scales.

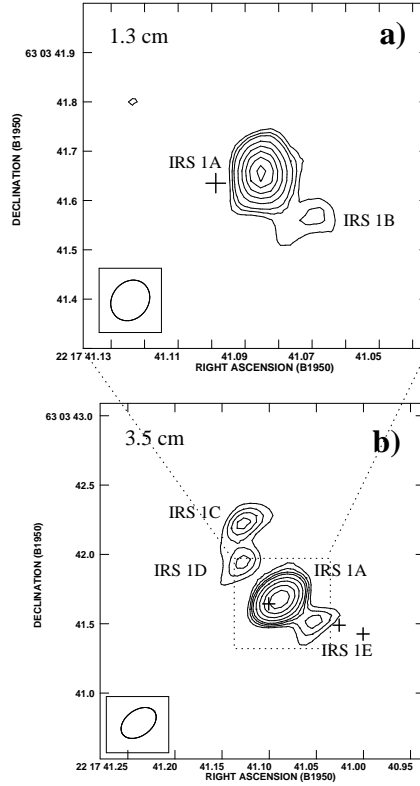


Fig. 2.— Multiple radio continuum sources detected toward S140 IRS 1A at different wavelengths. *a)* 1.3 cm continuum contour map. Contours are -3,3,4,5,7,9,11,13 and 15 times $230 \mu\text{Jy beam}^{-1}$, the rms noise of the map. The beam size is $0''.09 \times 0''.07$. *b)* 3.5 cm continuum contour map. Contours are -3,3,5,7,9,11,15,20,25 and 30 times $55 \mu\text{Jy beam}^{-1}$, the rms noise of the map. The beam size is $0''.29 \times 0''.20$. The crosses show the position of the water masers detected in the region.

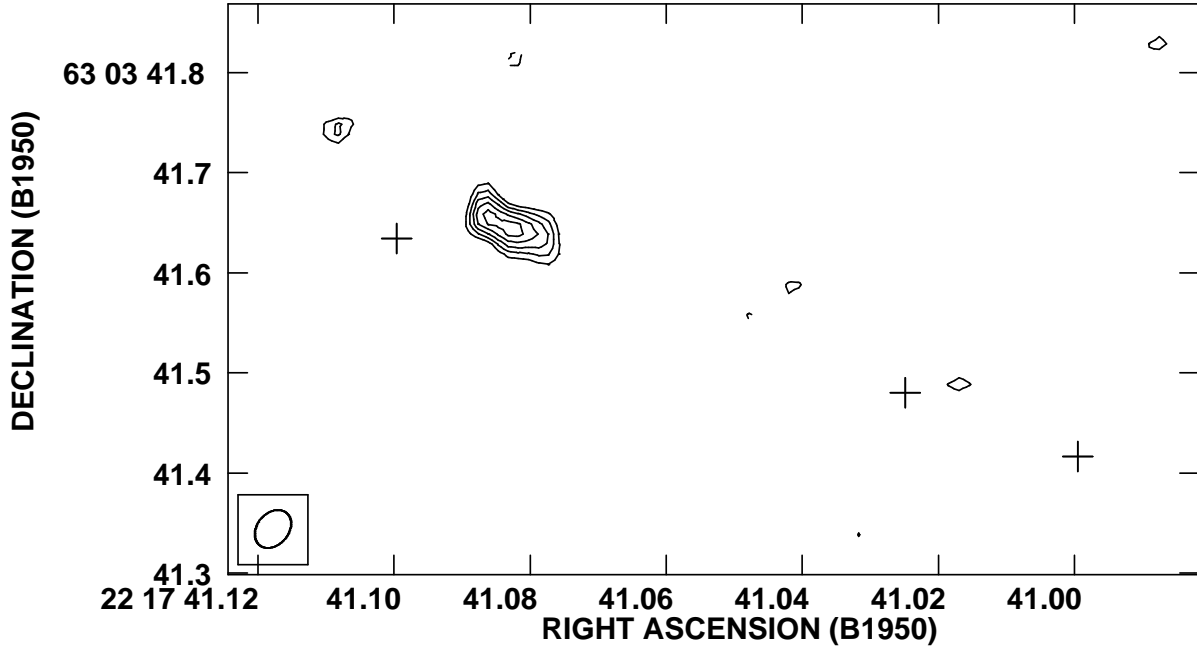


Fig. 3.— Contour map of S140 IRS 1A at 7 mm. Contours are $-3,3,4,5,6$ and 7 times $310 \mu\text{Jy beam}^{-1}$, the rms noise of the map. The beam size ($0''.04 \times 0''.03$) is shown in the lower left corner. The crosses show the position of the water masers observed toward the IRS 1A.

Table 1. Summary of the continuum observations toward S140 IRS 1

Wavelength (cm)	Observation Date	HPBW (arcsec)	Reference
0.7	1996 Nov 01	~ 0.04	VLA data archive (project AH5980)
1.3	1999 Jun 29	~ 0.1	This paper
2	1987 Sep 12	~ 0.1	Schwartz (1989)
3.5	1992 Nov 24	~ 0.3	Tofani et al. (1995)
6	1987 Sep 12	~ 0.3	Schwartz (1989)

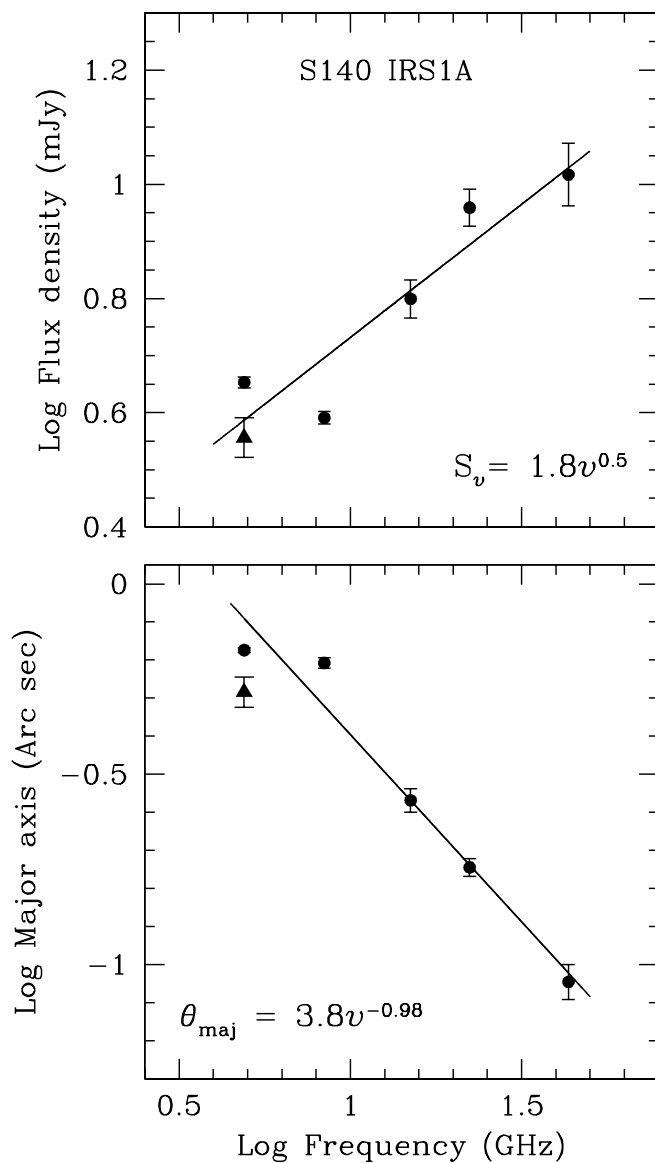


Fig. 4.— Flux density (top panel) and deconvolved angular size of the major axis (bottom) of IRS 1A are plotted as a function of frequency. The solid lines represent the least-squares fits from which the spectral indices α and β are obtained for IRS 1A. The filled triangles indicate the flux density (upper panel) and the size of the major axis (lower panel) of IRS 1 as obtained by Hoare (2006). These values were not used for the least-squares fits. The flux density, S_ν , is given in mJy, the frequency, ν , is given in GHz, and the deconvolved size of the major axis, θ_{maj} , is given in arcsec.

Table 2. Parameters of the continuum sources in S140 IRS 1

Source	Wavelength (cm)	Position ^a		Flux Density (mJy)	Angular Diameter
		$\alpha(1950)$	$\delta(1950)$		
IRS 1A	0.7	22 17 41.083	63 03 41.65	10.4±1.4	0′09 × 0′02; P.A. 61°
	1.3	22 17 41.083	63 03 41.64	9.1±0.7	0′18 × 0′08; P.A. 42°
	2	22 17 41.085	63 03 41.67	6.3±0.5	0′27 × 0′03; P.A. 45°
	3.5	22 17 41.091	63 03 41.70	3.9±0.1 ^b	0′62 × 0′11; P.A. 46°
	6	22 17 41.087	63 03 41.69	4.5±0.1	0′68 × 0′07; P.A. 41°
IRS 1B	1.3	22 17 41.070	63 03 41.57	0.92 ^c	< 0′08
IRS 1C	2	22 17 41.136	63 03 42.08	0.40 ^c	< 0′15
	3.5	22 17 41.128	63 03 42.24	0.45 ^c	< 0′2
IRS 1D	3.5	22 17 41.129	63 03 41.96	0.38 ^c	< 0′2
IRS 1E	3.5	22 17 41.045	63 03 41.53	0.38 ^c	< 0′2

^aUnits of right ascension are hours, minutes, and seconds, and units of declination are degrees, arcminutes, and arcseconds.

^bThis value is lower ($\sim 50\%$) than that reported by Tofani et al. (1995).

^cPeak flux density. The beam size is 0′09 × 0′07 at 1.3 cm, 0′16 × 0′14 at 2 cm, and 0′28 × 0′19 at 3.5 cm.

Table 3. Parameters of the water masers observed toward S140 IRS 1

Position ^a		V_{LSR} (km s ⁻¹)	Flux Density (Jy)
$\alpha(1950)$	$\delta(1950)$		
22 17 41.099	63 03 41.64	7.7	0.35
22 17 41.024	63 03 41.48	-16.0	2.29
22 17 40.999	63 03 41.42	-13.4	1.44

^aUnits of right ascension are hours, minutes, and seconds, and units of declination are degrees, arcminutes, and arcseconds.